Bonn nucleon-nucleon meson exchange model with a relativistic quark-gluon annihilation potential

J. Haidenbauer,* T. Hippchen,† and R. Tegen‡
Institut für Kernphysik (Theorie), Forschungszentrum Jülich, D-5170 Jülich, Germany
(Received 1 March 1991)

The full Bonn potential, combined with a relativistic quark-gluon annihilation potential, is compared with recent $N\bar{N}$ polarization data from LEAR and with measured differential cross sections (elastic and charge exchange) below $p_{\rm lab}=800$ MeV/c. It is demonstrated within this approach that a careful analysis of $p\bar{p}\to p\bar{p}$(EL) and $p\bar{p}\to n\bar{n}$(CEX), at the same energy, in terms of the five independent helicity amplitudes can be used to selectively test specific boson exchange contributions to $N\bar{N}$ scattering. The charge-exchange differential cross section in forward direction is particularly sensitive to the one-pion-exchange potential in this model. This feature could be used to see if recent attempts to fit NN data with a much softer πNN form factor can be made compatible with $N\bar{N}$ data.

I. INTRODUCTION

The Bonn meson exchange model for the nucleon-nucleon interaction [1] has recently been transformed to the nucleon-antinucleon interaction. We present here results of the Bonn $N\bar{N}$ potential combined with a quark-gluon annihilation potential, which was developed by one of us with Mizutani and Myhrer [2–4] several years ago. In Refs. [2,4–6] most of the well-known G-parity transformed nucleon-nucleon potentials had been tested, which are all given in r space ("local potentials"). The Bonn NN potential is given in momentum space ("nonlocal potential"); the unavoidable cutoffs in both local and nonlocal potentials acquire a *physical* meaning when transformed to momentum space: they are the well-known meson-nucleon form factors, which can be separately tested in subhadronic models (like chiral quark models and other subhadronic models). As an example let us consider the well-known pion-nucleon form factor, which is found in chiral quark models to be much softer (cutoff mass below 800 MeV [7,8]) than the same form factor used in NN scattering (cutoff mass in the range 1.3–1.5 GeV [1]). This ambiguity of the one-pion-exchange potential (OPEP) has recently been discussed by Holinde and Thomas [9]. They find that a much softer πNN form factor can indeed be made compatible with NN data if a pionlike π' with mass 1.2 GEV and a very large coupling strength is included. It remains to be seen whether such an additional π' (1200) exchange can be made compatible with $N\bar{N}$ data.

Since in configuration space the cutoff procedures adopted in NN scattering are *ad hoc* (usually involving many parameters), they do not allow "analytical continuation" to the $N\bar{N}$ case. One could, of course, argue in favor of these multiparameter fit procedures that the meson exchange approach is never under control at short NN distances, and, therefore, one might as well parametrize the short distance behavior all together. The $N\bar{N}$ interaction, in that picture, then does not provide complementary information, as it is further obscured by uncertainties in the annihilation potential (real *and* imaginary parts). In view of this it was surprising that the best known multiparameter model, the Paris $N\bar{N}$ potential [10], until recently had considerable difficulties in predicting the charge-exchange data at the forward angles. Both the Paris group and the Nijmegen group (who also use a multiparameter approach to $NN/N\bar{N}$ interactions [11]) now report better agreement with existing $N\bar{N}$ data after readjusting the "core parameters" of their models [10b, 11]. We want to adopt a different viewpoint in this paper. We believe that in order to get complementary and reliable information about the meson exchange picture from the $N\bar{N}$ system the consistency with the NN sector is very important. Furthermore, only in this case can a serious test of meson exchange dynamics at intermediate and short distances be achieved, which is essential for detecting possible effects of quark-gluon dynamics. In this context the Bonn NN potential is especially suited for such a study because the G-parity transformation connecting NN and $N\bar{N}$ dynamics can be applied in a well-defined way, without introducing any arbitrary parametrization of the inner part.

In this paper the G-parity transformed Bonn NN potential is combined with a purely imaginary one-parameter optical potential, which is based on a QCD inspired quark-antiquark annihilation model. Within this model we try to find systematics among the many possible meson exchange contributions, which stand out over and above the uncertainties related to the annihilation potential.

In a previous investigation [5] it turned out that a decomposition into the five independent helicity amplitudes revealed some interesting features of the $NN/N\bar{N}$-potential model at hand. The elastic (EL) and charge exchange (CEX) reactions are not only orthogonal isospin-0 and -1 combinations; in the forward direction the differential cross sections $d\sigma/d\Omega$ (EL) and $d\sigma/d\Omega$ (CEX) depend on (almost) complementary sets of helicity amplitudes [5]. We found within our approach that the CEX forward cross section is sensitive to the strength of ω and ρ exchange. The pronounced forward structure in $d\sigma/d\Omega$ (CEX) previously produced by the Paris potential [10a] (and its derivatives [12]) is not seen in the data [13] and possibly results from a too distorted one-pion ex-

change due to phenomenological cutoffs, which are also effective *above* 0.8 fm (see our discussion above and Ref. [6]). These difficulties seem to have been overcome now, as reported in [10b]. None of the other investigated models (Nijmegen model *D* [11], Bryan-Phillips model [14], and black sphere annihilation model [5]) shows this behavior. A careful analysis of the Bonn potential in terms of helicity amplitudes is given below.

In the following section we briefly discuss the Bonn potential and the quark-gluon annihilation model. Results and discussions are presented in Sec. III, which is followed by our conclusions.

II. THE BONN POTENTIAL AND THE QUARK-GLUON MODEL

A comprehensive overview of the Bonn NN potential can be found in Ref. [1]. Our present investigations are based on the full model as it is defined in Table 9 therein. This interaction model includes not only traditional one-boson-exchange (OBE) diagrams but furthermore explicit uncorrelated 2π- and $\pi\rho$-exchange processes involving nucleons as well as Δ isobars in the intermediate states. The single σ' exchange corresponds here, in a well-defined way, to the correlated 2π-exchange S-wave contributions—in contradistinction to the fictitious σ meson commonly used in OBE NN models—which accounts not only for effects from 2π but also from $\pi\rho$ exchange. This aspect is very important when we go over to the $N\bar{N}$ system, i.e., when we apply the G-parity transformation. Since the $\pi\rho$ contributions enter with different signs in the NN and $N\bar{N}$ systems, respectively, they cancel to some extent with the 2π part for NN but add up for $N\bar{N}$. Thus we get considerably more attraction in the $N\bar{N}$ interaction derived from the full Bonn potential as compared to OBE models because there the common assignment of positive G parity to $\sigma_{\rm OBE}$ leads to the same (attractive) contributions for both systems.

Another salient feature of the Bonn potential becomes apparent when it comes to the treatment of the short-range domain. The pointlike meson-baryon vertices are furnished with form factors in order to appropriately take into account the extended structure of the hadrons. These form factors are parametrized via cutoff masses and provide the necessary suppression of the high-momentum components in the interaction. As a consequence, the G-parity transform can be applied in a clear-cut manner and arbitrary modifications or *ad hoc* regularizations of the inner part (often introduced in other $N\bar{N}$ models) can be avoided.

The potential described so far, however, provides (after G-parity transformation), only the elastic part of the $N\bar{N}$ interaction. Due to the presence of annihilation channels, one has to supplement it with an optical potential in order also to take into account these processes, so that we finally have

$$V_{N\bar{N}} = V_{\rm el} + V_{\rm opt} \ . \tag{2.1}$$

In general, $V_{\rm opt}$ will contain both a real and an imaginary part due to the second iteration of annihilation processes (which contain real and imaginary parts)

$$V_{\rm opt} = U_{N\bar{N}} + iW_{N\bar{N}} \ . \tag{2.2}$$

Here we will use only an imaginary optical potential, i.e., $U_{N\bar{N}} \equiv 0$. The reason is partly to avoid unnecessary fit parameters and partly based on our finding in [2–4,6] that different annihilation diagrams [with one, two, or three timelike gluons (Fig. 1) and any number of spacelike bremsstrahlung gluons] all contribute with the same sign to $W_{N\bar{N}}(0)$ but with alternating signs to $U_{N\bar{N}}(0)$; extracting the real part from annihilation diagrams in dynamical models is therefore problematic, and we will take in Eq. (2.2) only $W_{N\bar{N}}(r)$ from a dynamical annihilation model, derived within a QCD approach to $N\bar{N}$ annihilation. The neglect of $U_{N\bar{N}}$ in (2.2) in this paper receives further support from the analysis in Ref. [15], where a phenomenological, complex, spin-isospin and energy-independent optical potential of Gaussian form

$$V_{\rm opt}(r) = (U_0 + iW_0)\exp(-r^2/2R^2)$$

was employed. The free parameters U_0, W_0, and R were determined by a fit to $N\bar{N}$ data below $p_{\rm lab} = 800$ MeV/c with the result $U_0 = -0.63$ GeV, $W_0 = -4.567$ GeV, and $R = 0.36$ fm. This result shows clearly that U_0 is very much smaller than W_0, in agreement with the finding in Refs. [2–4,6].

In the following we describe the basic steps in obtaining $W_{N\bar{N}}(r)$, Eq. (2.2). We have calculated in Ref. [3] the r dependence of the processes (Fig. 1)

$$N\bar{N} \rightarrow \left\{ \begin{matrix} qqG\bar{q}\bar{q} \\ qGG\bar{q} \\ GGG \end{matrix} \right\} \rightarrow N\bar{N} \tag{2.3}$$

in terms of a quark-antiquark correlation function $\rho(r)$ (henceforth called "annihilation density") on the basis of the chiral bag model or the Dirac-Scalar potential model [2–4,6,7]. To derive $\rho(r)$ we showed in certain approxi-

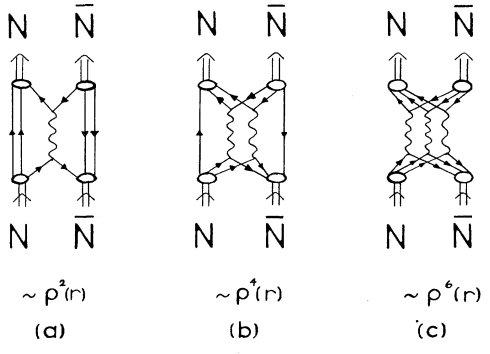

FIG. 1. Quark-line diagram for $N\bar{N} \rightarrow N\bar{N}$. (a) One $q\bar{q}$-annihilations into a timelike gluon. (b) Two $q\bar{q}$-annihilations into two timelike gluons. (c) Three $q\bar{q}$-annihilations into three timelike gluons. This is a quark-line disconnected diagram, suppressed in agreement with the Okubo-Zweig-Iizuka rule; see the text. Soft ("bremsstrahlungs") gluons are not shown.

mations (closure or coherent approximation for bound fermions) that the number of *timelike* gluons determines the *dominant* quark-line diagrams. The more $q\bar{q}$ pairs that annihilate, the shorter the annihilation range [3]. The spacelike gluons (bremsstrahlung) contribute only to the overall strength but do not strongly modify the r dependence of the basic diagrams. These results were obtained within a "sudden approximation," i.e., the internal q ($\bar{q}$) wave function of the nucleon (antinucleon) are not modified until $q\bar{q}$ annihilation occurs. This approximation should work best at higher energies. We also assume that on the average the timelike gluon's momentum is $|\mathbf{k}|\simeq 0$, whereas $k_0=E_q+E_{\bar{q}}$, the sum of the quark and antiquark energies. Note that our assumption is the same as in the $^3P_0$ model, where $\mathbf{k}\equiv 0$ holds [16]. We neglect spin-dependent parts, which are specific for the one-$q\bar{q}$ annihilation diagram. The reason is that bremsstrahlung gluons will wash out all spin dependence originating from the basic $q\bar{q}$-gluon vertex. This idea is also expressed in statistical thermodynamical descriptions of $p\bar{p}$ annihilation; see the discussion in Ref. [5b]. The same reasoning is applied to the two-$q\bar{q}$ pair and three-$q\bar{q}$ pair annihilation diagrams. This is in the spirit of the $^3P_0$ model, where $q\bar{q}$ pairs annihilate "into the vacuum." The r dependence of the fundamental $q\bar{q}$-gluon annihilation vertex differs from that of the $^3P_0$ model in one important aspect: the vertex function is (in configuration space)

$$\bar{v}\left[\mathbf{y}+\frac{\mathbf{r}}{2}\right]\gamma^{\mu}\frac{\lambda_a}{2}u\left[\mathbf{y}-\frac{\mathbf{r}}{2}\right], \tag{2.4}$$

where u and v are solutions of the bound Dirac equation

$$[i\partial_x^{\mu}\gamma_{\mu}-M(x)]u(x)=0=[i\partial_y^{\mu}\gamma_{\mu}+M(y)]v(y)$$

with the confinement coordinates (the time-dependent part of u,v is $e^{\pm iEt}$, as usual) $\mathbf{x}=\mathbf{r}_1-\mathbf{r}/2$, $\mathbf{y}=\mathbf{r}_1+\mathbf{r}/2$, and the confining potential $M(x)=c|\mathbf{x}|^n$ ($n=2,3$ see Ref. [17]). Note that quark and antiquark have different confinement centers, which are a distance $\mathbf{r}$ apart, therefore we make the ansatz (2.4), which is distinct from the $^3P_0$ model. The ansatz (2.4) leads to a form factor [2],

$$F_a^{\mu}(\mathbf{k};\mathbf{r})=\int d^3y\, e^{-i\mathbf{k}\cdot\mathbf{y}}\langle\bar{v}(\mathbf{y})\gamma^{\mu}(\lambda_a/2)u(\mathbf{y}-\mathbf{r})\rangle ,$$

which simplifies for the $^3P_0$ ansatz ($\mathbf{k}=0$) to

$$\begin{aligned} &F_a^{\mu=0}(\mathbf{k}=0;\mathbf{r})=0 ,\\ &F_a^{\mu=j}(\mathbf{k}=0;\mathbf{r})\sim\rho(r)\langle\sigma^j\lambda_a/2\rangle \quad (j=1,2,3) , \end{aligned} \tag{2.5}$$

where $\rho(r)$ is totally determined by the solutions u,v of the Dirac equation, see Ref. [2]. In Fig. 2 we have plotted $\rho(r)$ for a core radius of 0.55 fm. Also shown are the Wood-Saxon potential used in Refs. [12,14,16] (with parameters adjusted to fit $N\bar{N}$ data in conjunction with the elastic $N\bar{N}$ interaction employed in the present study), and the Gaussian form [given after Eq. (2.2)], used in Ref. [15]. Clearly, the annihilation potential based on quark-gluon dynamics is distinct from the phenomenological Wood-Saxon form; it has an r-dependent "range," which is independently fixed by comparison to axial-vector form factor data of the nucleon [7]. On the other hand, the

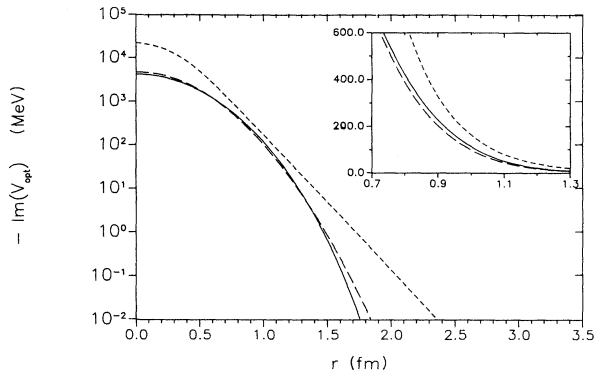

FIG. 2. Annihilation potential vs relative distance of N and $\bar{N}$, Eq. (2.2). Note that all models produce values of ~ 100 MeV in the vicinity of $r=1$ fm.

Gaussian form comes very close to the quark-gluon model; thus it can be regarded as an excellent phenomenological representation of more fundamental annihilation dynamics. Note that all models roughly agree at $r=1$ fm, with a potential strength of ~ 100 MeV. This feature is obviously necessary for a good overall reproduction of $N\bar{N}$ data and has been pointed out already by Dover and Richard [12]. Averaging out the spin dependence in (2.5) then finally gives the remarkable result

$$W_{N\bar{N}}(r)=\epsilon_2\rho^2(r)+\epsilon_4\rho^4(r)+\epsilon_6\rho^6(r) , \tag{2.6}$$

where $\epsilon_{2,4,6}$ are spin-isospin and energy-averaged constants [2–4,6]. Color matrix elements prefer ϵ_2 over $\epsilon_{4,6}$, and $p\bar{p}$ observables are insensitive (at the percent level) to the region $0\le r\le 0.5$ fm; this means that the much shorter-ranged terms $\rho^4(r)$ and $\rho^6(r)$ in Eq. (2.6) do not influence $p\bar{p}$ observables). (Note that the ρ^6 term [Fig. 1(c)] corresponds to a quark-line disconnected diagram, which according to the Okubo-Zweig-Iizuka rule should be suppressed; our calculation shows the dynamical origin of this suppression for the $p\bar{p}$ case [2–4].) We therefore use

$$W_{N\bar{N}}(r)=\epsilon_2\rho^2(r)=W_0\rho^2(r) \tag{2.7}$$

instead of (2.6) and leave W_0 as a parameter to be determined by fitting $p\bar{p}$ elastic and charge-exchange data [4].

III. RESULTS AND DISCUSSIONS

With the annihilation model, Eq. (2.7), combined with several meson exchange models (Bryan-Scott model, Nijmegen model D, and Dover-Richard model) it was found in [4] that $W_0\simeq -2$ GeV; this defines an annihilation scale, which is much more natural than the phenomenological annihilation scale (-8.3 and -20 GeV) set by Wood-Saxon parametrizations of $W_{N\bar{N}}(r)$ [12,14,16]. In Figs. 3 and 4 we compare the Bonn $N\bar{N}$ potential combined with $W_{N\bar{N}}(r)$, Eq. (2.7), with elastic and charge exchange (CEX) $d\sigma/d\Omega$ at $p_{\mathrm{lab}}=490,690$ MeV/c. We have investigated in particular the forward structure in

CEX at 690 MeV/c; this forward structure is mainly due to an interference of the φ_2 and φ_4 helicity amplitude [see Fig. 4(b)]. The no-net helicity flip amplitude φ_2 (we use Yokosawa's notation [18]) is largest at $\theta=0$ and falls exponentially between 0° and 60°, while the double-flip helicity amplitude φ_4 rises from zero at $\theta=0$ to a maximum around $\theta=40°$ and decreases again. The other helicity amplitudes $\varphi_{1,3,5}$ are less important in forward direction. We confirm *qualitatively* Shibata's finding [22] that the CEX forward cross section is mainly due to one-pion exchange ($\varphi_{2,4}$). Any modification of the one-pion-exchange (like the soft form factor model suggested recently by Holinde and Thomas [9]) should therefore be tested also in this reaction, $p\bar{p}\to n\bar{n}$. For a *quantitative* fit to CEX data in forward directions, however, the heavier meson exchanges (ρ,ω,σ') are essential. The analysis in terms of helicity amplitudes $|\varphi_1|,\ldots,|\varphi_5|$ shows that the magnitude of $|\varphi_2|$ and $|\varphi_4|$ in forward directions is essentially given by one-pion exchange; adding on heavier meson exchanges leaves $|\varphi_2|$ and $|\varphi_4|$ remarkably stable. This is *not* so for $|\varphi_1|$ and $|\varphi_3|$; these amplitudes are approximately a factor of 5 smaller than the leading $|\varphi_2|$ and $|\varphi_4|$ amplitudes in forward directions. Their relative magnitude determines how well the forward dip between 10° and 20° (originating from the $\varphi_2-\varphi_4$ interference, which is mainly due to one-pion exchange) is filled in. Data do *not* indicate a forward dip, which implies large contributions from $\varphi_{1,3}$. Considering only one-pion exchange in the Bonn potential we find that $|\varphi_3|$ is a factor of 4 smaller than the leading $|\varphi_2|$ in forward directions, but $|\varphi_1|$ is even larger than $|\varphi_3|$, unlike the full model, which produces $|\varphi_1|$ always smaller than $|\varphi_3|$. Adding on successively heavier meson exchanges leaves $|\varphi_1|$ relative to $|\varphi_{2,4}|$ stable, while $|\varphi_3|$ wildly fluctuates; starting from one-pion-exchange we find $|\varphi_1|$ larger than $|\varphi_3|$ for the π exchange and ($\pi+\sigma'$) exchange and for the ($\pi+\omega$) exchange, while the inclusion of the ρ exchange reserves the order of $|\varphi_1|$ and $|\varphi_3|$ drastically. The full model then again has $|\varphi_1|$ smaller than $|\varphi_3|$, which is mainly due to ($\pi+\rho$) exchange effects. It is clear from our helicity analysis that a larger $|\varphi_3|$ amplitude (larger than is observed for the full model) would yield less structure in CEX forward directions; this situation is realized if we only use the OBE sector of the full Bonn potential as elas-

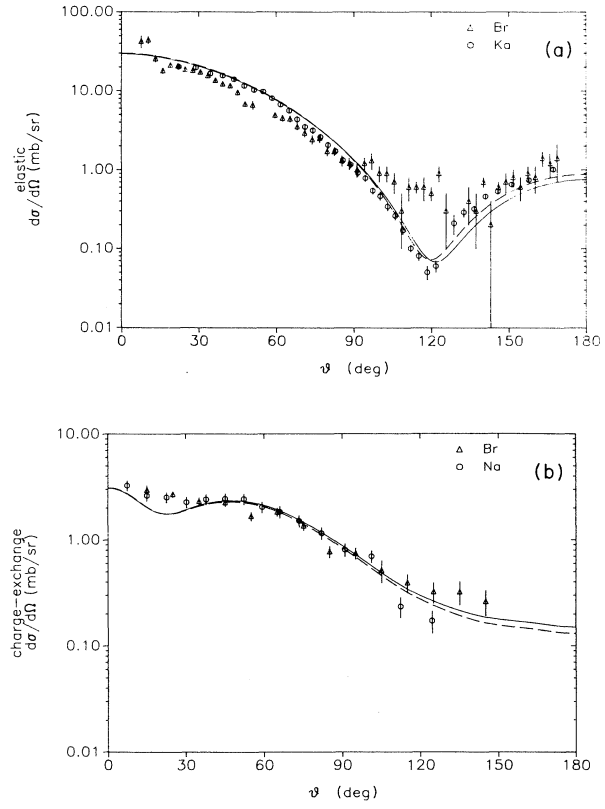

FIG. 3. Comparison of the full Bonn potential with two different annihilation potentials: the Gaussian form, given after Eq. (2.2) (dashed); quark-gluon annihilation potential, Eq. (2.7), with $W_0=-4$ GeV and a quark core radius of 0.55 fm (solid). (a) $(d\sigma/d\Omega)_{\rm EL}$ with two data sets: LEAR [19] (△) and KEK [20] (○) at $p_{\rm lab}=505$ and 490 MeV/c, respectively. (b) $(d\sigma/d\Omega)_{\rm CEX}$ with two data sets: LEAR [21] (△) at $p_{\rm lab}=505$ MeV/c and KEK [13] (○) at $p_{\rm lab}=490$ MeV/c.

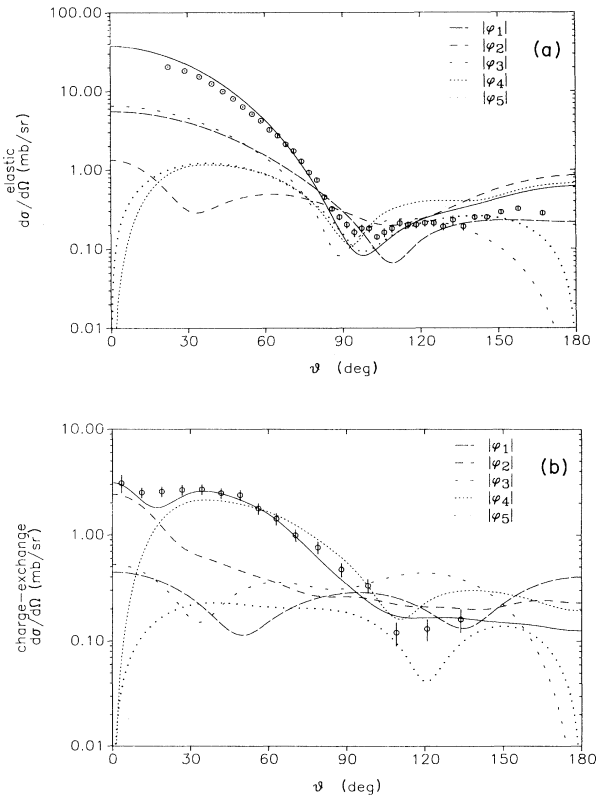

FIG. 4. (a) $(d\sigma/d\Omega)_{\rm EL}$ at $p_{\rm lab}=690$ MeV/c; data are from KEK [20]. The different curves show the five helicity amplitudes, as indicated; they correspond to the annihilation potential, Eq. (2.7). (b) $(d\sigma/d\Omega)_{\rm CEX}$ at $p_{\rm lab}=690$ MeV/c; data are from KEK [13]. Otherwise as in (a).

tic part in the calculations. There the $|\varphi_3|$ amplitude is appreciably larger than the $|\varphi_1|$ amplitude in the dip region. It must be noted, however, that $\varphi_{1,3}$ are dominant in forward directions of the elastic cross-section, and any imbalance of φ_1 and φ_3 will have different effects in CEX and EL. Corresponding results can be seen in Fig. 5, where we compare CEX and EL for $p_{\rm lab}=690$ MeV/c.

The helicity analysis for other models was done in Ref. [5]; the Dover-Richard model [12] produces generally too much forward structure in $(d\sigma/d\Omega)_{\rm CEX}$ due to very small amplitudes $|\varphi_{1,3}|$. They also find $|\varphi_3|>|\varphi_1|$ in forward directions. As mentioned in the Introduction, the readjusted Paris $N\bar{N}$ potential produces much less structure in the forward direction [10(b)]. How the new parameter set affects the different helicity amplitudes is presently unknown. The "black sphere" annihilation model [5], on the other hand, produces no structure in the forward direction due to very large $|\varphi_{1,3}|$ (comparable to $|\varphi_2|$) in forward directions; this model has $|\varphi_1|>|\varphi_3|$. It is interesting to note that the Dover-Richard model, combined with a quark gluon annihilation model (without a real part), has $|\varphi_3|$ essentially unchanged, while $|\varphi_1|$ is now appreciably larger than $|\varphi_3|$. This indicates to us that the helicity analysis can be used in CEX to selectively study various meson exchanges with their associated parameters in $|\varphi_1|$ and $|\varphi_3|$. Although we have here applied the helicity analysis only to the Bonn potential, this technique might also be useful for the fine-tuning of parameters in the multiparameter $NN/N\bar{N}$ models. The elastic reaction at the same energy has $\varphi_{1,3}$ dominant in forward directions and should be used as a check for the (varied) model. This is important for the recently revived interest in the "good old" one-pion exchange [9]. The NN data seem to be compatible now with a much softer πNN form factor (as soft as is found in chiral quark models [7,8]) at the cost of introducing a pionlike exchange π' (1200) with mass above 1 GeV. The corresponding modification in $\mathrm{ReU}_{N\bar{N}}$, Eq. (2.1), can be tested in the forward structure in $(d\sigma/d\Omega)_{\rm CEX}$ [23]. Another observation is that even relatively high partial waves give non-negligible contributions to the forward structure of the CEX cross section. In general, it was necessary to include all partial waves up to $J=12$ in order to get convergent results. In Fig. 6 we compare our model with three different data sets (KEK [24], LEAR [25], and the old CERN data of Eisenhandler *et al.* [26]) between $p_{\rm lab}=780$ and 790 MeV/c. The KEK data are essentially flat between 100° and 180°, in conflict with the old CERN data [26], which show the onset of a dip-bump structure; the LEAR data show more structure at backward angles than the KEK data. On the theoretical side, the onset of a dip-bump structure as a function of increasing $p_{\rm lab}$ is determined by the quark core radius [which determines the radial dependence of the annihilation potential $W_{N\bar{N}}(r)$]; the smaller the quark core radius the later the onset of the backward structure. The quark core radius also plays a role in determining the *height* of the forward shoulder in the CEX reaction. The smaller the quark core the higher the forward shoulder; the Bonn $N\bar{N}$ potential when combined with Eq. (2.7) is much less sensitive to variations of the quark core radius than other models [4]. This might be due to the nonlocalities in the Bonn potential.

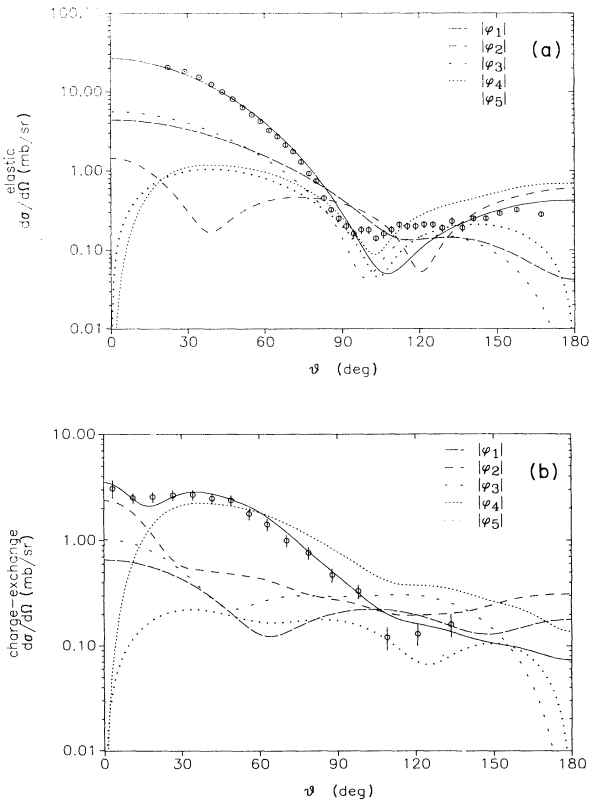

FIG. 5. (a) $(d\sigma/d\Omega)_{\rm EL}$ at $p_{\rm lab}=690$ MeV/c. Data are from KEK [20]. Curves correspond to the OBE sector of the full Bonn potential combined with the annihilation as in Eq. (2.7); otherwise as in Fig. 4(a). (b) $(d\sigma/d\Omega)_{\rm CEX}$ at $p_{\rm lab}=690$ MeV/c. Data are from KEK [13]; otherwise as in (a).

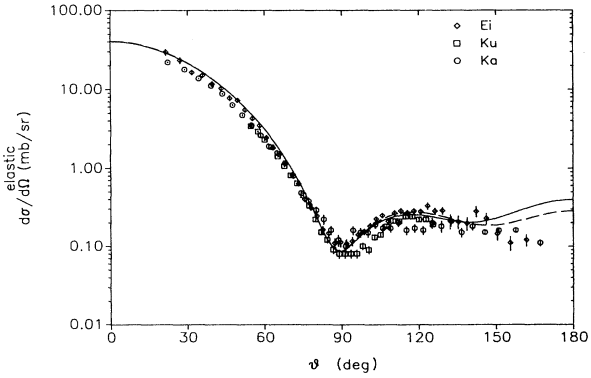

FIG. 6. $(d\sigma/d\Omega)_{\rm EL}$ at $p_{\rm lab}=780$ MeV/c. Curves are as in Figs. 3(a) and 3(b). Data are from CERN [26] (◇), LEAR [25] (□), and KEK [20] (○) at $p_{\rm lab}=790$, 783, and 780 MeV/c, respectively.

As was discussed in Sec. II, it turned out that the purely phenomenological annihilation potential of Gaussian form used in Ref. [15] is quite a good approximation to the annihilation model derived within a QCD approach in [2–6] and employed in the present investigation. It is therefore interesting to compare $N\bar{N}$ observables predicted by these two models. We included some curves obtained with the Gaussian annihilation form in Figs. 3, 6, and 7. Not surprisingly, the results are very similar, especially in forward direction. There are, however, distinct differences for backward angles, for both the elastic as well as the CEX cross sections. Clearly, these variations come from discrepancies (in the radial dependence) of the two annihilation models, since exactly the same input was used for the elastic part. This is, in fact, in agreement with earlier results reported in Refs. [2–6], where a strong sensitivity of the backward (elastic) cross section to the imaginary part of the optical potential has been found.

Finally, we show predictions of these two models for recently measured $N\bar{N}$ analyzing powers [27,28], for both the elastic [Fig. 7(a)] and the charge-exchange [Fig. 7(b)] channels. For the elastic case small differences occur mainly around 90°. In the CEX reaction they appear more in the backward region and are also somewhat more pronounced.

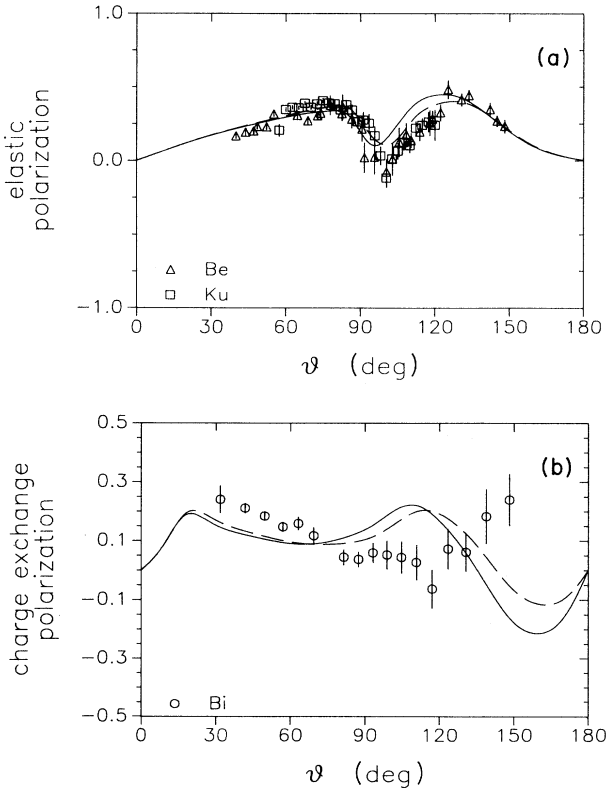

FIG. 7. Polarization vs scattering angle θ; curves as in Figs. 6(a) and 6(b). (a) EL at $p_{\rm lab}=679$ MeV/c [Ref. [25] (□)] and $p_{\rm lab}=697$ MeV/c [Ref. [28] (△)]. (b) CEX at $p_{\rm lab}=656$ MeV/c. Data are from Ref. [27].

IV. CONCLUSION

Nucleon-nucleon scattering can seemingly be understood without quarks and gluons as evidenced again, recently, by the extremely successful multiparameter NN and $N\bar{N}$ models. The quark picture, however, enters through the regularization procedures/meson-nucleon form factors. One might ask if there is more direct evidence for quarks and gluons in nucleon-*antinucleon* scattering. The optical potential for $N\bar{N}$ scattering has an imaginary part due to the opening of physical annihilation channels $N\bar{N}\to n\pi(n=5\pm1)$ so that again a field theoretic model involving baryons and mesons might ultimately succeed in explaining the annihilation. The meson- *antibaryon* form factors, however, emerge from the fitting procedures in a different form from those obtained from NN fits. From a QCD point of view, this feature finds a natural explanation: while even nonrelativistic quark models reproduce basic features of meson-nucleon form factors, the meson-antibaryon form factors can *only* be derived in *relativistic* quark-gluon models where the fundamental quark-antiquark annihilation vertex into gluon(s) is a *natural* ingredient of the underlying QCD Lagrangian. The phenomenological annihilation strength is of order 2–4 GeV much smaller than in Wood-Saxon parametrizations. The presence of the annihilation in the optical potential does *not* wash out the cutoff dependence in both local and nonlocal $N\bar{N}$ models. Moreover, we find that some observables are selectively sensitive to Re $V_{N\bar{N}}$ (derived from NN) and Im$V_{N\bar{N}}$ (annihilation part). There seems to be growing evidence that the real part of the annihilation potential is considerably weaker than the imaginary part; acceptable fits can be obtained even with a vanishing real annihilation potential, provided the radial dependence of the imaginary part provides for a sufficient annihilation strength at a distance of 0.8–1.0 fm.

While the CEX differential cross sections are sensitive in forward directions to the annihilation potential, the elastic cross sections display such sensitivity mainly at the backward angles. The CEX $d\sigma/d\Omega$ in forward direction is sensitive to both W_0 and the size of the quark core radius; a larger (smaller) core radius reduces (increases) the height of the forward structure (shoulder), whereas a larger (smaller) W_0 makes the forward structure more (less) pronounced. The Bonn $N\bar{N}$ potential when combined with the quark-gluon annihilation potential is much less sensitive to variations of the quark core radius than other models. The elastic $d\sigma/d\Omega$ is particularly sensitive to the imaginary part in the backward direction. Without annihilation, $d\sigma_{\rm EL}/d\Omega$ would peak at the backward angle $\theta=180°$. If one considers the experimental $d\sigma_{\rm EL}/d\Omega$ as a function of $p_{\rm lab}$ then a dip-bump structure develops at $p_{\rm lab}>690$ MeV/c; the position of the dip moves to smaller angles θ as $p_{\rm lab}$ is increased ("antishrinkage"). This trend is clearly displayed in the old CERN data of Eisenhandler *et al.* Recent LEAR and KEK data, however, show no dip-bump structure below 780 MeV/c. This is not a minor issue because the onset of the dip-bump structure as a function of increasing $p_{\rm lab}$ is determined by the magnitude of the

quark core radius (which determines the radial dependence of the annihilation potential); the *smaller* the quark core radius, the *later* the onset of the backward structure. It is therefore important to remove the discrepancy among different experiments between $p_{\rm lab} \simeq 700$ and 800 MeV/c.

Concerning the form of the annihilation vertex we find a preference for some aspects of the $^3P_0$ model ("annihilation into a vacuumlike state") and find little evidence for a $^3S_1$ vertex structure, due mainly to the presence of infinitely many soft bremsstrahlung gluons, which completely wash out the spin and color structure of the vertex. Three classes of annihilation diagrams emerge; timelike ("hard") and bremsstrahlung ("soft") gluons behave differently. To further study this behavior, we suggest studying explicit channels like $N\bar{N} \to \pi\pi, K\bar{K}$. Only for these channels have differential cross sections been measured for $0° \leq \theta \leq 180°$.

Available $N\bar{N}$ data are now of a quality comparable to NN experiments (see in particular the accurate polarization data from LEAR). However, further (and other) spin observables would be necessary for a competitive phase shift analysis of $N\bar{N}$ scattering where the number of partial waves is much larger than for NN scattering (where they are limited by the Pauli principle).

We have emphasized here that the helicity analysis of $p\bar{p} \to p\bar{p}$ and $p\bar{p} \to n\bar{n}$ at the same energy, can be used to selectively test specific boson (or two bosons as in box diagrams) exchange contributions to $N\bar{N}$ scattering in the Bonn $N\bar{N}$ potential. This technique could be useful for removing the remaining ambiguity of the good old one-pion exchange. Recently Holinde and Thomas have restricted the πNN form factor (inherent in OPE) to be as soft as was found in chiral quark models (cutoff mass below 800 MeV) at the cost of including a π' with mass 1.2 GeV and a very large coupling constant. Such modifications of the OPE in NN scattering should show up in forward CEX $d\sigma/d\Omega$ predominantly in the helicity amplitudes φ_2 and φ_4. Work along this line is in progress.

---

*Present address: Department of Physics and Mathematical Physics, University Adelaide, P.O. Box 498, Adelaide, South Australia 5001, Australia.

†Now at Ford GmbH, Köln, Germany.

‡Permanent adddress: University of the Witwatersrand, Physics Dept., Johannesburg 2050, South Africa.

[1] R. Machleidt *et al.*, Phys. Rep. **149**, 1 (1987) and references to earlier papers of the Bonn group cited therein.

[2] R. Tegen, T. Mizutani, and F. Myhrer, Phys. Rev. D **32**, 1672 (1985).

[3] F. Myhrer and R. Tegen, Phys. Lett. **162B**, 237 (1985).

[4] R. Tegen, F. Myhrer, and T. Mizutani, Phys. Lett. B **182**, 6 (1986).

[5] (a) T. Mizutani, F. Myhrer, and R. Tegen, Phys. Rev. D **32**, 1663 (1985); (b) C. Amsler and F. Myhrer, Annu. Rev. Nucl. Part. Sci. **41**, 1 (1991).

[6] R. Tegen, in *Proceedings of the International Workshop on Quarks, Gluons and Hadronic Matter, Cape Town, 1987,* edited by R. D. Viollier (World Scientific, Singapore, 1987), pp. 354–395.

[7] R. Tegen and W. Weise, Z. Phys. A **314**, 357 (1983).

[8] J. Speth and R. Tegen, Nucl. Phys. **A511**, 716 (1990).

[9] K. Holinde and A. W Thomas, Phys. Rev. C **42**, R1195 (1990).

[10] (a) J. Coté, M. Lacombe, B. Loiseau, B. Moussallam, and R. Vinh Mau, Phys. Rev. Lett. **48**, 1319 (1982); (b) M. Pignone *et al.*, *Proceedings of the 1st Biennial Conference on Low Energy Antiproton Physics, Stockholm, 1990,* edited by P. Carlson *et al.* (World Scientific, Singapore, 1991), p. 90.

[11] P. H. Timmers *et al.*, Phys. Rev. D **29**, 1928 (1984).

[12] J. M. Richard, M. Lacombe, and R. Vinh Mau; Phys. Lett. B **64**, 121 (1976); C. B. Dover and J. M. Richard, Phys. Rev. C **21**, 1466 (1980).

[13] K. Nakamura *et al.*, Phys. Rev. Lett. **53**, 885 (1984).

[14] R. A. Bryan and R. J. N. Phillips, Nucl. Phys. **B5**, 201 (1968).

[15] J. Haidenbauer *et al.*, Z. Phys. A **334**, 467 (1989).

[16] C. B. Dover, in *Proceedings of the International Symposium on Medium Energy Nuclear and Antinuclear Science Bad Honnef, 1985,* edited by H. V. von Geramb, Lecture Notes in Physics, Vol. 243 (Springer-Verlag, Berlin, 1985), p. 80.

[17] R. Tegen, Phys. Lett. **172B**, 153 (1986); Phys. Rev. Lett. **62**, 1724 (1989); in *Proceedings of the International Symposium on Weak and Electromagnetic Interactions in Nuclei, Heidelberg, 1986,* edited by H. V. Klapdor (Springer-Verlag, Berlin, 1986), pp. 548–552.

[18] A. Yokosawa, Phys. Rep. **64**, 47 (1980).

[19] W. Brückner *et al.*, Phys. Lett. **166B**, 113 (1986).

[20] T. Kageyama *et al.*, Phys. Rev. D **35**, 2655 (1987).

[21] W. Brückner *et al.*, Phys. Lett. **169B**, 302 (1986).

[22] T. A. Shibata *et al.*, Phys. Lett. B **189**, 232 (1987).

[23] J. Haidenbauer *et al.* (unpublished).

[24] T. Tanimori *et al.*, Phys. Rev. Lett. **55**, 1835 (1985).

[25] R. Kunne *et al.*, Nucl. Phys. **B323**, 1 (1989); Phys. Lett. **206B**, 557 (1988).

[26] E. Eisenhandler *et al.*, Nucl. Phys. **B113**, 1 (1976).

[27] R. Birsa *et al.*, Phys. Lett. B **246**, 267 (1990).

[28] R. Bertini *et al.*, Phys. Lett. B **228**, 531 (1989); F. Perrot-Kunne *et al.*, in *Proceedings of the 1st Biennial Conference on Low Energy Antiproton Physics, Stockholm, 1990,* edited by P. Carlson *et al.* (World-Scientific, Singapore, 1991).